Estimation of Atmospheric Temperature Using Microwave Radar

Marshall Bradley
LogLinear Group, LLC
28 December 2015

Introduction

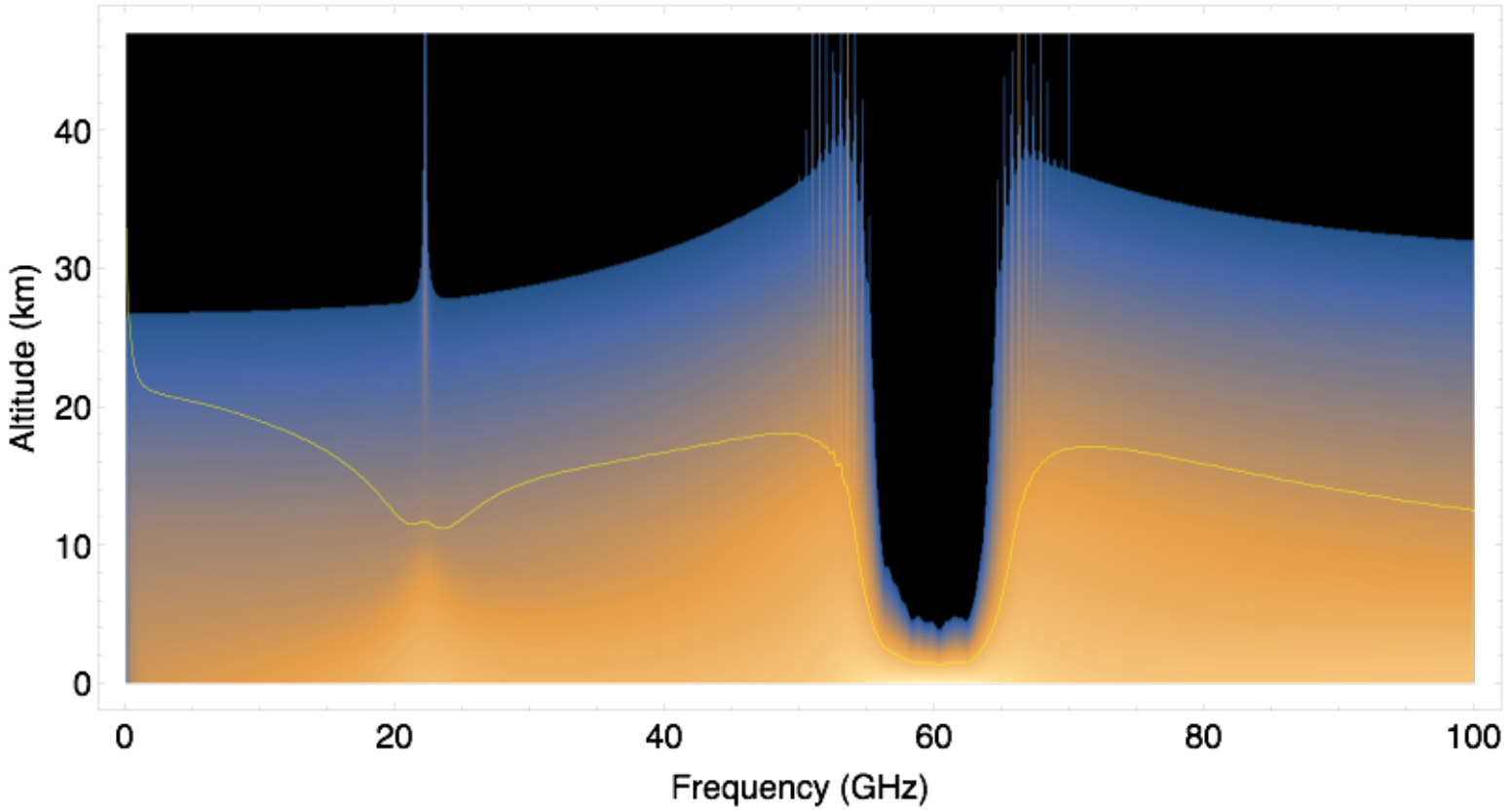

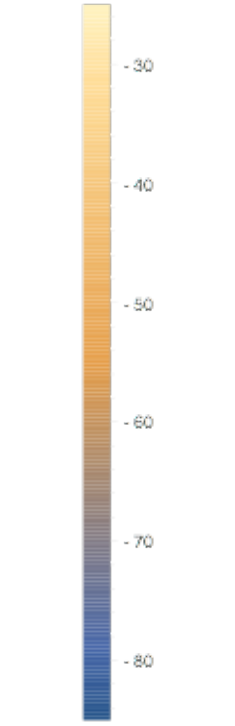

Discussion. In December of 2015 it was experimentally observed that the LLG radar could make an accurate measurement of the dependence of received background noise energy as a function of radar tilt angle. This measurement closely agreed with a theoretical calculation of this quantity using a standard atmosphere. This experiment was successfully repeated on the 9th of December with the radar operating both in active and passive mode. This immediately suggests that the radar can be used to measure the variation of temperature as a function of altitude in addition to measuring wind velocity. That portion of the noise energy budget that the radar receives from the troposphere and beyond is referred to as the brightness temperature (T^{bright}). The relationship between T^{bright} and the vertical profile of temperature in the atmosphere $T(z)$ is described by the equation shown to the right. In this equation $\alpha_\nu(z)$ denotes absorption at frequency ν. Although not indicated here, absorption depends upon temperature, pressure and moisture. The figure above shows how the environmentally dependent portion of this relationship varies with altitude and frequency. The yellow line shows the 99th percentile of received energy as a function of frequency. Figure generated by "*Fast Tropospheric Noise Temperature. nb*".

$$T_\nu^{bright} = \int_0^\infty T(z)\alpha_\nu(z) e^{-\int_0^z \alpha_\nu(\xi)\,d\xi}\,dz$$

http://demonstrations.wolfram.com/AtmosphericRadarWaveAbsorption/

Sky noise observed on 7 December 2015

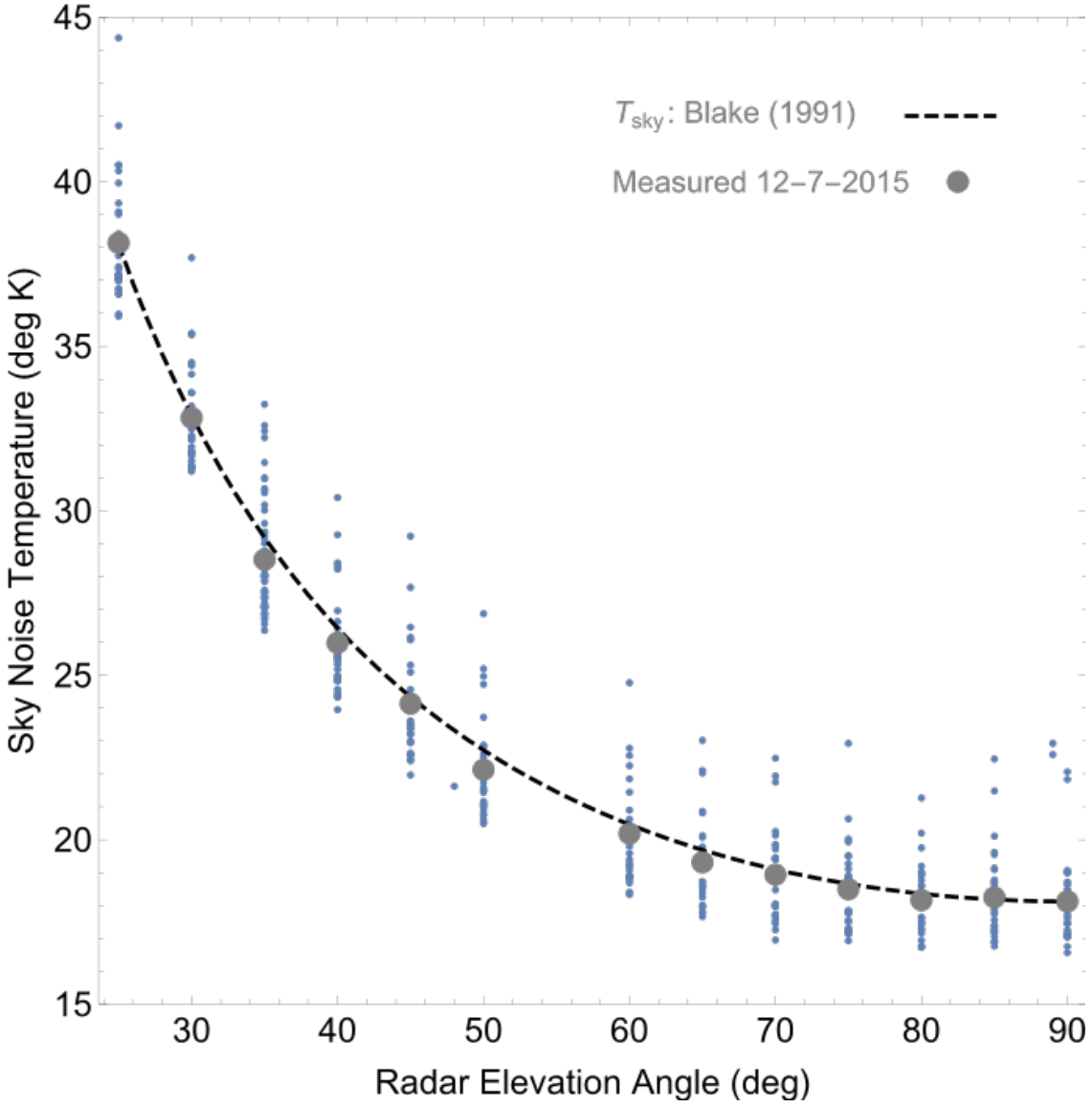

http://demonstrations.wolfram.com/NoiseTemperatureOfARadarSystem/

Discussion. Measured sky noise values made with the LLG-QNA radar on 7 December 2015 at the Stennis International Airport. Data were collected from 1658 to 2103 Z. Sky noise is noise observed by the radar that comes from the troposphere (0-47 km) and the cosmos (beyond 47 km for ordinary radar frequencies). The range of radar elevation angles in the figure is 25-90 degrees with 90 degrees corresponding to the vertical (radar looking straight up). At 33.4 GHz the cosmos contribution to sky noise is 2.5 deg K and is very nearly independent of elevation angle over the range 25-90 deg. Thus sky noise in this case is effectively tropospheric noise. Smaller points in the plot indicate individual radar sky noise measurements. Larger gray points indicate mean values. Estimations of the sky noise temperature using algorithms from Blake (1991) are shown for reference via the dashed black line. Computations with the Blake algorithms for the sky noise temperature have been made using on scene measurements of atmospheric temperature and pressure. Sky noise temperature is lowest near the vertical because at these angles the radar beam trajectory spends the least amount of time in the denser portions of the atmosphere which occur at lower altitudes. The data in the figure indicate a radar total system noise temperature of 130 deg K at an elevation angle of 90 degrees. It had previously been estimated that the radar system noise temperature was 300 deg K. However this data-model comparison provides a more accurate radar calibration than previous estimates based only upon system parameters. Figured generated using *"Radar Vertical Tilt Data Analysis 7*

Side by side

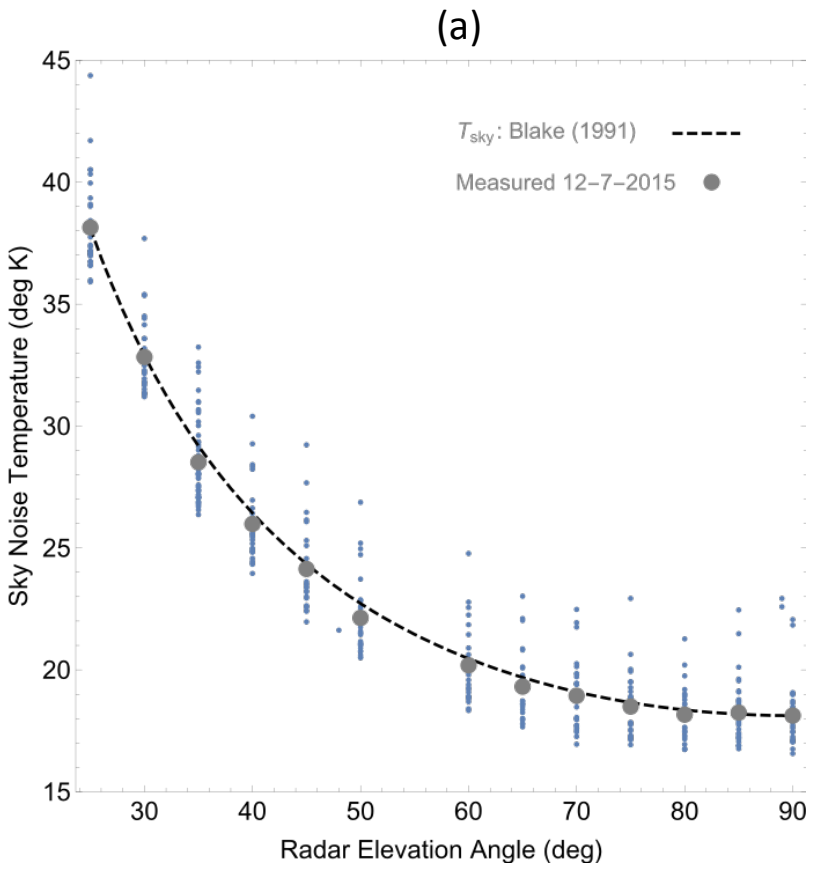
(a)
T_{sky}: Blake (1991)
Measured 12–7–2015
Sky Noise Temperature (deg K)
Radar Elevation Angle (deg)
45
40
35
30
25
20
15
30
40
50
60
70
80
90

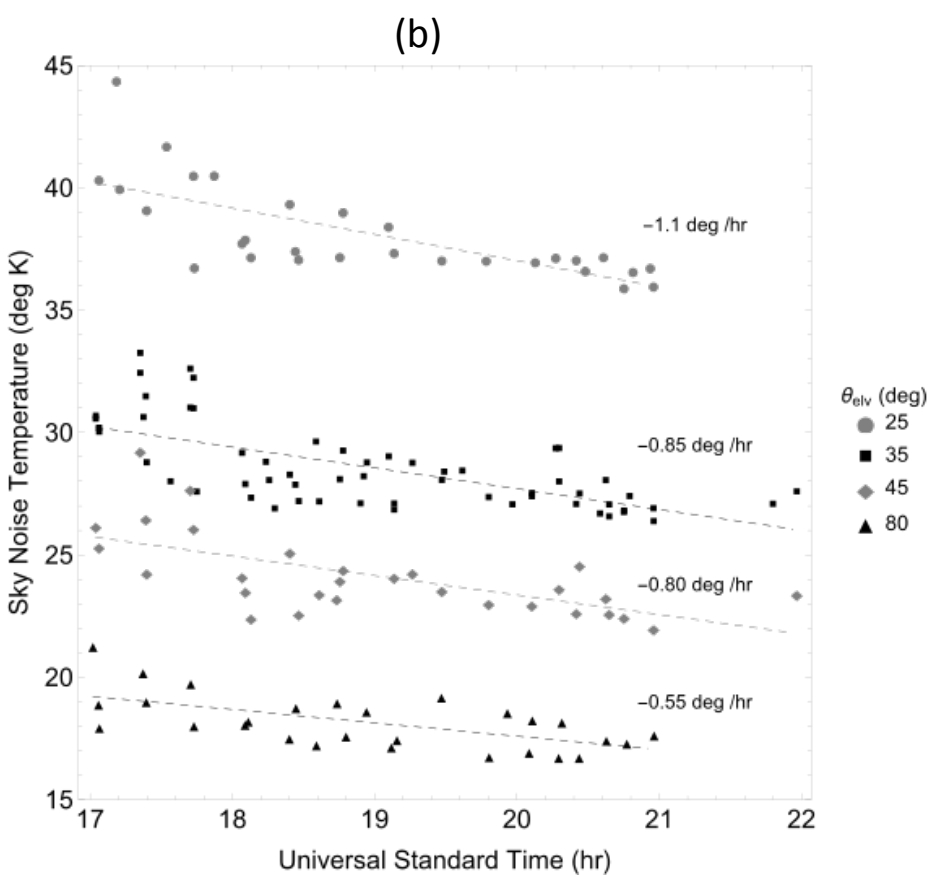
(b)
−1.1 deg /hr
−0.85 deg /hr
−0.80 deg /hr
−0.55 deg /hr
Sky Noise Temperature (deg K)
Universal Standard Time (hr)
θ_{elv} (deg)
25
35
45
80
45
40
35
30
25
20
15
17
18
19
20
21
22

Time variation of sky noise ()observed on 7 December 2015

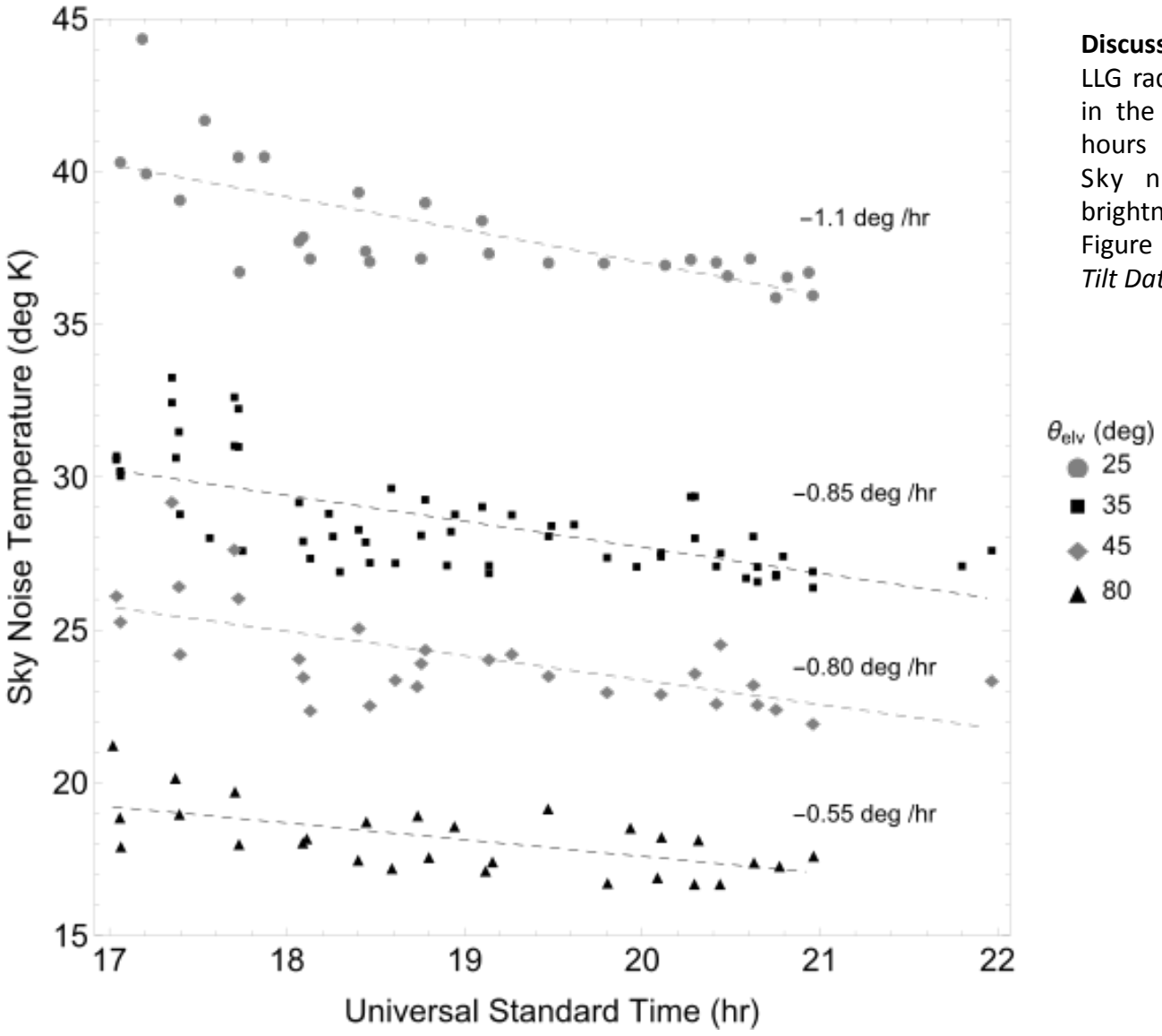

Discussion. This figure indicates that the LLG radar can track temperature trends in the atmosphere over the course of hours and across multiple tilt angles. Sky noise is also referred to as brightness temperature in this brief. Figure generated using "*Radar Vertical Tilt Data Analysis 7 December 2015*".

Time variation of noise floor LLNL on 18-20 February 2015

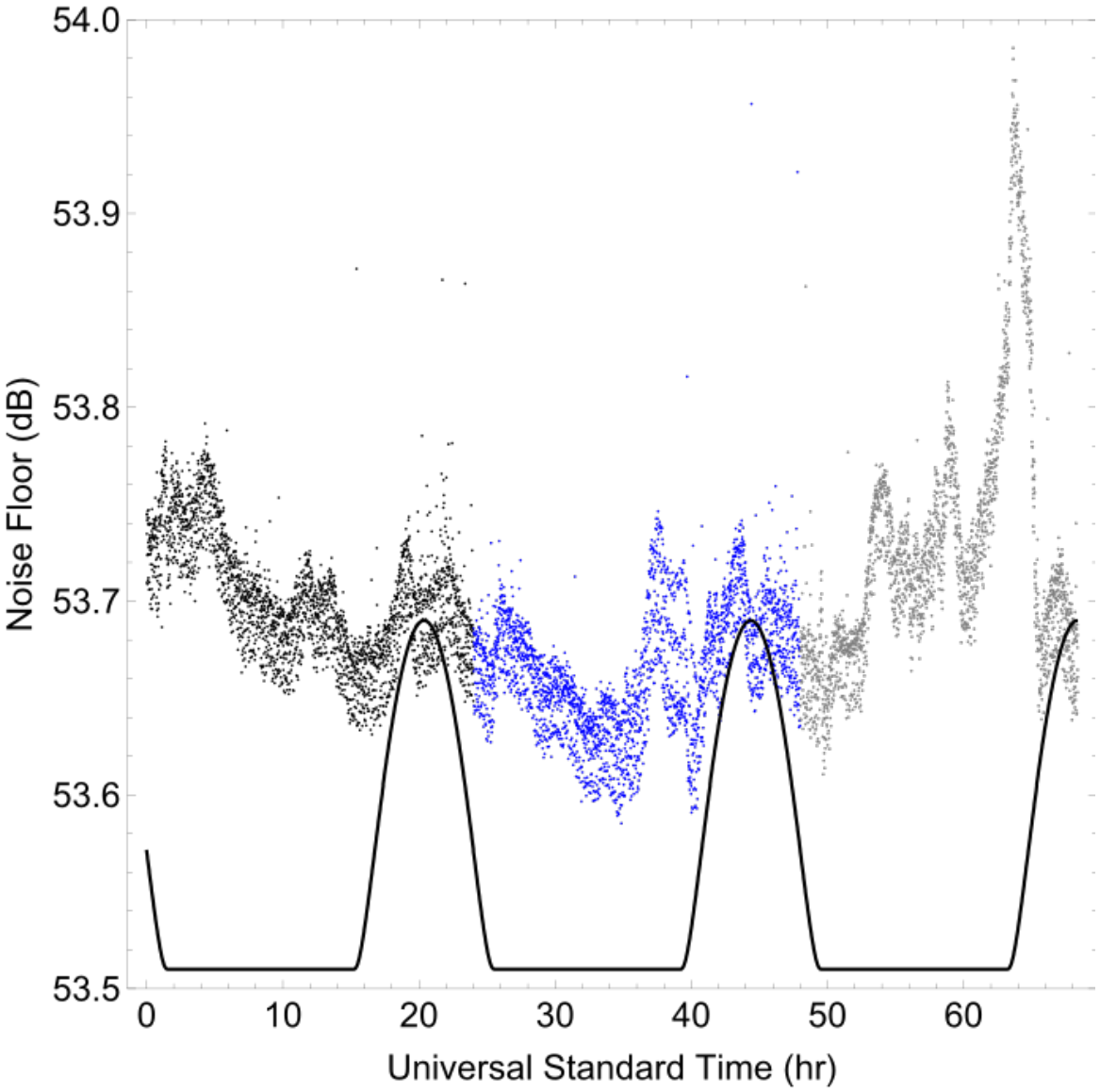

Discussion. This figure indicates that the LLG radar can track temperature trends in the atmosphere over the course of days and observe correlations with solar activity. The figure also indicates there are effects in play other than solar activity also. Figure generated using "*Solar Effects Lawrence Livermore 2015*.nb".

Visualizing the construction of a cubic spline

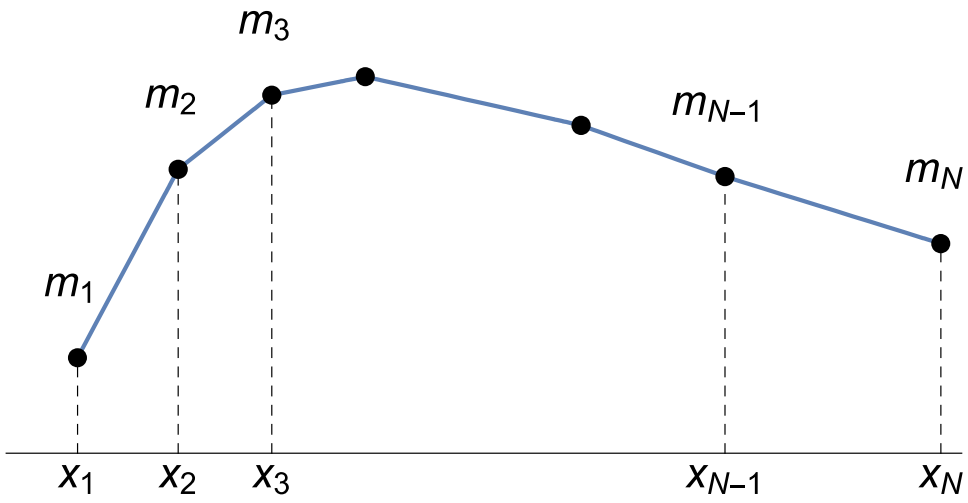

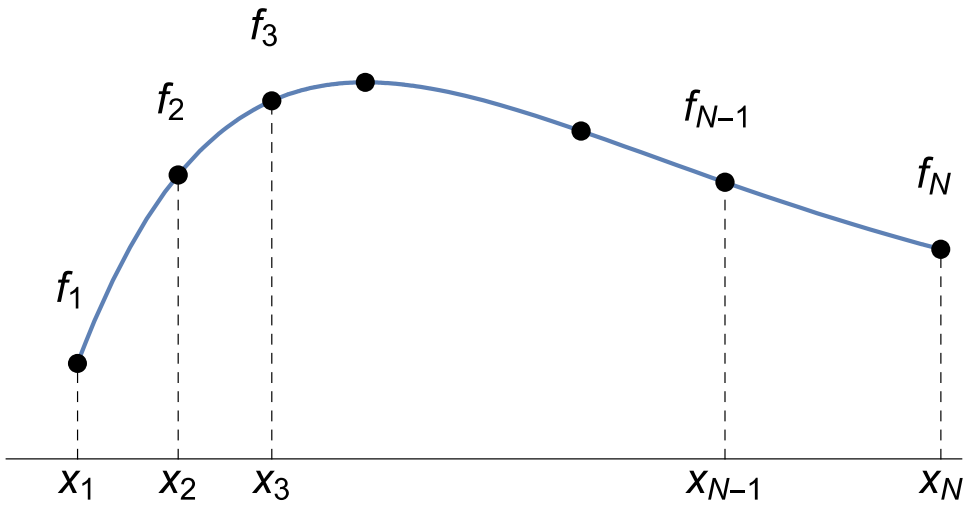

Discussion. The construction of a cubic spline representation for a function $f(x)$ begins with representing the second derivative of $f(x)$ as a piecewise continuous linear function. In the figure shown to the left the values of the second derivative of $f(x)$ at the lattice points x_j, j=1,2,..,N are denoted by m_j with h_{j+1} defined to be $h_{j+1}=x_{j+1}-x_j$. The second derivative of this function on the interval $x_j \le x \le x_{j+1}+1$ is

$$S_j''(x) = m_j + \frac{m_{j+1}-m_j}{h_{j+1}}(x-x_j)$$
$$= \frac{x_{j+1}-x}{h_{j+1}} m_j + \frac{x-x_j}{h_{j+1}} m_{j+1}$$

In writing the preceding equation we have used $S(x)$ is an alternative name for $f(x)$. Integrating $d^2S(x)/dx^2$ twice yields a cubic polynomial that has global curvature on the interval (x_1,x_N) that is smaller than any other twice continuously differential function on this interval. The results of these two integrations are shown in the lower figure to the left. The points (x_j, f_j) are referred to as the control points (or the pivot points) of the spline. Concept adapted from von der Linden (2014). Figures generated by "*Spline Global Smoothness Figures*.nb".

Reference: Adapted from von der Linden, W., Dose, V. and von Toussaint, U. (2014), *Bayesian Probability Theory: Applications for the Physical Sciences*, (Cambridge: Cambridge University Press).

Analytic representation of a cubic spline

$$S_j(x) = \frac{m_{j+1}h_{j+1}^2}{6}\left[\left(\frac{x-x_j}{h_{j+1}}\right)^3 - \left(\frac{x-x_j}{h_{j+1}}\right)\right] + \frac{m_j h_{j+1}^2}{6}\left[\left(\frac{x_{j+1}-x}{h_{j+1}}\right)^3 + \left(\frac{x-x_j}{h_{j+1}}\right) - 1\right] + f_{j+1}\left(\frac{x-x_j}{h_{j+1}}\right) + f_j\left(\frac{x_{j+1}-x}{h_{j+1}}\right)$$

Discussion. Integrating the second derivative of $S(x)$ twice and application of the requirement that $S(x)$ must pass through the points (x_j,f_j) and (x_{j+1},f_{j+1}) for j=2,3,…,N-1 leads to the representation of the cubic spline $S(x)$ shown in the equation above. At this point we know the pivot abscissas x_j and the their spacings h_j. The values of the pivot ordinates f_j and their second derivatives m_j are unknown. Continuity of the first derivative of $S(x)$ at the points (x_j,f_j) for j=2,3,…,N-1 supplies N-2 equations. The requirement that the second derivative of $S(x)$ is zero at x_1 and x_N leads to the equations shown to the left and above and produces a form of spline that is referred to as a natural spline. Natural splines are terminated at inflection points. The rather formidable collection of equations shown to the right express the second derivatives of $S(x)$ in terms of the known functional values f_j and the pivot point abscissas x_j together with their spacings h_j. At this point the only unknowns are the pivot point ordinates f_j. They must be found from data or other information.

$$\mathbf{M}_{N\times N}.\mathbf{m}_{N\times 1} = \mathbf{F}_{N\times N}\mathbf{f}_{N\times 1}$$

where

$$\mathbf{m} = \{m_1, m_2, \ldots, m_N\}^T$$

$$\mathbf{f} = \{f_1, f_2, \ldots, f_N\}^T$$

$$\mathbf{m}_{N\times 1} = \mathbf{L}_{N\times N}\mathbf{f}_{N\times 1}$$

$$\mathbf{L}_{N\times N} = \mathbf{M}^{-1}_{N\times N}\mathbf{F}_{N\times N}$$

$$\mathbf{M}_{N\times N} = \frac{1}{6}\begin{bmatrix} 2h_2 & 0 & & \\ h_2 & 2(h_2+h_3) & h_3 & \\ \ldots\ldots & h_{N-2} & 2(h_{N-1}+h_N) & h_N \\ & & 0 & 2h_N \end{bmatrix}$$

$$\mathbf{F}_{N\times N} = \begin{bmatrix} 0 & 0 & & \\ \frac{1}{h_2} & -\frac{h_2+h_3}{h_2 h_3} & \frac{1}{h_3} & \\ \ldots\ldots & \frac{1}{h_{N-1}} & -\frac{h_{N-1}+h_N}{h_{N-1}h_N} & \frac{1}{h_N} \\ & & 0 & 0 \end{bmatrix}$$

Note. The symbols x and f in the above equations will respectively correspond to altitude and atmospheric temperature elsewhere in this presentation.

Reference: Adapted from von der Linden, W., Dose, V. and von Toussaint, U. (2014), *Bayesian Probability Theory: Applications for the Physical Sciences*, (Cambridge: Cambridge University Press).

Forward model of radiative transfer

LOGLINEAR GROUP

Discussion. In order to begin the process of estimating the atmospheric vertical temperature profile from observed radar brightness temperatures we first must mathematically relate these quantities via a form that lends itself to numeric computation. To this end we represent the atmospheric temperature profile $T(z)$ via a cubic spline. In terms of the preceding discussion x represents and altitude and f represents temperature. The first thing we must do is choose a set of pivot point abscissas $(x_1,x_2,\ldots x_N)$ such the first abscissa correspond to the ground (x=0)and the last abscissa corresponds to an altitude above which there is negligible contribution to the radar brightness temperature from the atmosphere. If we repeat this process for each frequency (or radar tilt angle) for which data has been collected, the result is a matrix equation relating the observed brightness temperatures to the unknown pivot point ordinates: $\mathbf{y}=\mathbf{A}\mathbf{f}$. The matrix $\mathbf{A}$ is known as the forward matrix. It relates the atmospheric temperatures in the vector $\mathbf{f}$ that we would like to know to the brightness temperatures $\mathbf{y}$ that we have measured. A very naïve thing to do at this point would be to make an estimate of the unknown vector $\mathbf{f}$ using the familiar least squares solution $\mathbf{f}^{(LS)}=(\mathbf{A}^T\mathbf{A})^{-1}\mathbf{A}^T\mathbf{y}$. The problem here is that the matrix $\mathbf{A}^T\mathbf{A}$ is very ill conditioned with numerous small eigenvalues and only a few eigenvalues (if any) that are significantly different from zero. The solution that results from the naïve least squares approach will bear no semblance to reality, even in the absence of of measurement noise. It is at this point that a Bayesian approach which incorporates prior knowledge about the atmospheric temperature profile becomes vital. In fact it is only in a Bayesian context that solutions to a problem like this make any sense at all.

$$T_\nu^{bright} = \int_0^\infty T(x)\alpha_\nu(x) e^{-\int_0^x \alpha_\nu(\xi)\,d\xi}\,dx$$

$$T(x) \rightarrow S_j(x \mid f_j, m_j),\ j = 1,2,\ldots,N$$

$$T_\nu^{bright} = \sum_{j=1}^{N} a_{\nu j} f_j$$

$$a_{\nu j} = \int_0^\infty S_j(x \mid f_j, m_j)\alpha_\nu(x) e^{-\int_0^x \alpha_\nu(\xi)\,d\xi}\,dx$$

$$\mathbf{T}^{bright}_{N_d \times 1} = \mathbf{y}_{N_d \times 1} = \mathbf{A}_{N_d \times N}\mathbf{f}_{N \times 1}$$

N = number of pivot points

N_d = number of measurements

Likelihood of data and posterior distribution of pivots

LOGLINEAR GROUP

Discussion. The likelihood of obtaining the measured brightness temperature data **y** given the forward matirix **A** and the values of the pivot point ordinates **f** on initial information *I* is given by the top equation shown to the right. The pivot abscissas **x** are taken to part of the initial information *I*. In the experimental examples that follow, measurement errors will be assumed to be uncorrelated and the measurement error covariance matrix $\mathbf{C}_\sigma$ will be assumed to be diagonal with diagonal elements σ_i, i,1,2,…,N_d. We will additionally assume that these diagonal elements are identical with value 4 deg K. On initial information I we will assume that the initial values of the pivot ordinates follow an N_d dimensional normal distribution with mean $\mathbf{f}_a$ given in accordance with the Blake standard atmosphere and with uncertainty measured by the covariance matrix $\mathbf{S}_a$ shown to the right (Rogers, 2012). In the equation defining the covariance matrix values, δx is a length scale that we take to be the distance between the first two pivot point abscissas and $h_{cor}=-\delta x/\log\beta$ is a correlation distance. In this matrix $\beta=0.95$. According to Rodger,s this choice of parameters provides some modeling of the inner level correlations that probably exist in the atmosphere.

Bayes theorem tells us that the posterior distribution of the pivot points **f** in light of the measured data is given by the fourth equation shown to the right. In this equation Z_{const} is a normalization constant. In order to make computations tractable we will assume that our measurement errors and our prior knowledge about the pivot point ordinates are both normally distributed. In this case the posterior distribution p(**f**|**y**,**A**,I) is also normally distributed and we can obtain useful information about the pivot point ordinates without resorting to intensive numerical computations. Specifically the mean $\mathbf{f}_{mean}$ and covariance $\mathbf{C}_\mathbf{f}$ of the posterior distribution of **f** are given by the last of the two equations shown to the right.

$$p(\mathbf{y}\mid\mathbf{A},\mathbf{f},I)=\frac{1}{\Pi_{i=1}^{N_d}\sigma_i\sqrt{2\pi}}\exp\left[-\frac{1}{2}\left(\mathbf{y}-\mathbf{A}\mathbf{f}\right)^T\mathbf{S}_\sigma^{-1}\left(\mathbf{y}-\mathbf{A}\mathbf{f}\right)\right]$$

$$p(\mathbf{f}\mid\mathbf{f}_a,\mathbf{S}_a,I)=\frac{1}{\Pi_{j=1}^{N}\sigma_a^2\sqrt{2\pi}}\exp\left[-\frac{1}{2}\left(\mathbf{f}-\mathbf{f}_a\right)^T\mathbf{S}_a^{-1}\left(\mathbf{f}-\mathbf{f}_a\right)\right]$$

$$S_{a,ij}=\sigma_a^2\exp\left(-\mid i-j\mid\frac{\delta x}{h_{cor}}\right)$$

$$p(\mathbf{f}\mid\mathbf{y},\mathbf{A},I)=\frac{1}{Z_{const}}p(\mathbf{y}\mid\mathbf{A},\mathbf{f},I)p(\mathbf{f}\mid\mathbf{f}_0,\mathbf{S}_a,I)$$

$$\mathbf{f}_{mean}=\mathbf{f}_a+(\mathbf{A}^T\mathbf{S}_\sigma^{-1}\mathbf{A}+\mathbf{S}_a^{-1})^{-1}\mathbf{A}^T\mathbf{S}_\sigma^{-1}(\mathbf{y}-\mathbf{A}\mathbf{f}_a)$$

$$\mathbf{C}_\mathbf{f}=(\mathbf{A}^T\mathbf{S}_\sigma^{-1}\mathbf{A}+\mathbf{S}_a^{-1})^{-1}$$

Reference: Rogers, C.D. (2004), *Inverse Methods for Atmospheric Sounding: Theory and Practice* (Hackensack: World Scientific Publishing).

Obtaining a solution through a process of iteration

Discussion. The technique for obtaining a solution for the temperature pivot ordinates **f** described in the previous slide produces an initial estimate $\mathbf{f}_1$ In order to obtain a final estimate, an iterative procedure of refinement must be used. This results from the fact that absorption in the atmosphere depends on temperature, pressure and water vapor density. Because of this, at each stage of the refinement the forward matrix **A** must be updated using the new temperature profile. This essentially corresponds to a re-computation of the data depicted in the color figure in the introduction slide. Pressure is estimated from a standard gas law: $p(x)=p_0\{\exp(-[g/(R_{gas}T(x))]x\}$ where $p(x)$ is pressure at altitude x, g is the acceleration due to gravity, $T(x)$ is temperature at altitude x and R_{gas} is a gas constant with value 287 MKs units. In order to initialize the process, the individual entries in the forward matrix **A** in the examples that follow were computed using values of temperature, pressure and water vapor density for the Blake (1991) standard atmosphere. Typically about 4-7 iterations of this procedure are required to reach convergence.

Test cases. We now consider two test cases. The first of these is based upon data reported by Westwater (1965) in Dakar. Westwater's data were actually measured on 2 February 1956. They were recorded with a vertically oriented radiometer operating over the band 45-57 GHz. These data correspond to the rapidly changing region of absorption shown in the introductory slide. The second data set is the measurements made on 7 December 2015 by LLG at 33.4 GHz with the radar at elevation angles in the range 25- 90 deg. Atmospheric temperature profiles were measured with a radiosonde for both data sets.

Test case 1: Dakar 2 February 1956

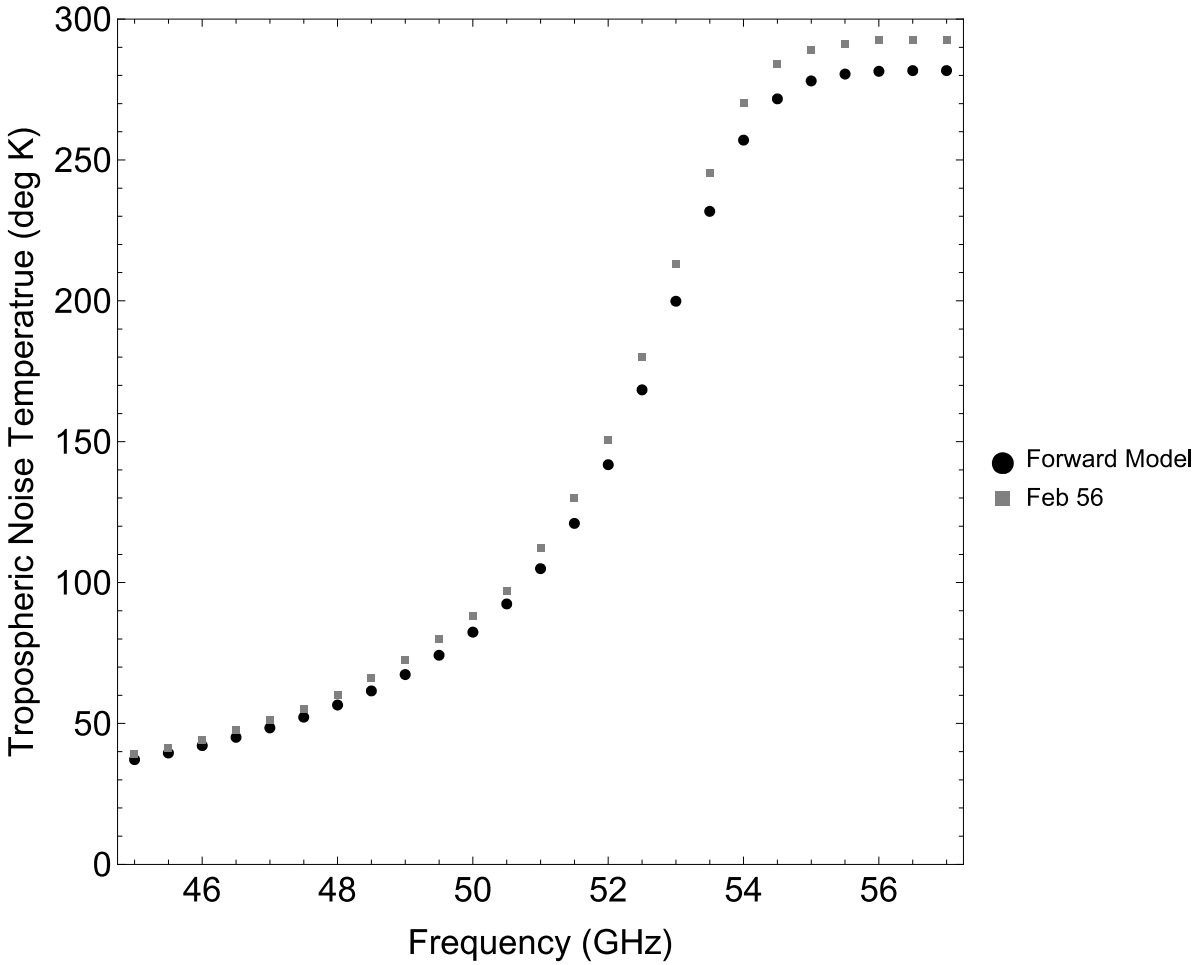

Discussion. The gray squares in the figure above are Westwater's data for Dakar on 2 February 1956. Note that the variation of brightness temperature between 45 and 57 GHz is approximately 250 deg K. Also shown in the figure is the forward computation of the brightness temperature using the measured temperature from 2 February 1956. Figure generated using " *Brightness Temperature Dakar Senegal 2 February 1956 Actual Data.nb*".

Reference: Westwater, E. R. (1965). "Ground Based Passive Probing Using the Microwave Spectrum of Oxygen", Radio Science, Vol 69D, September 1965.

Side by side

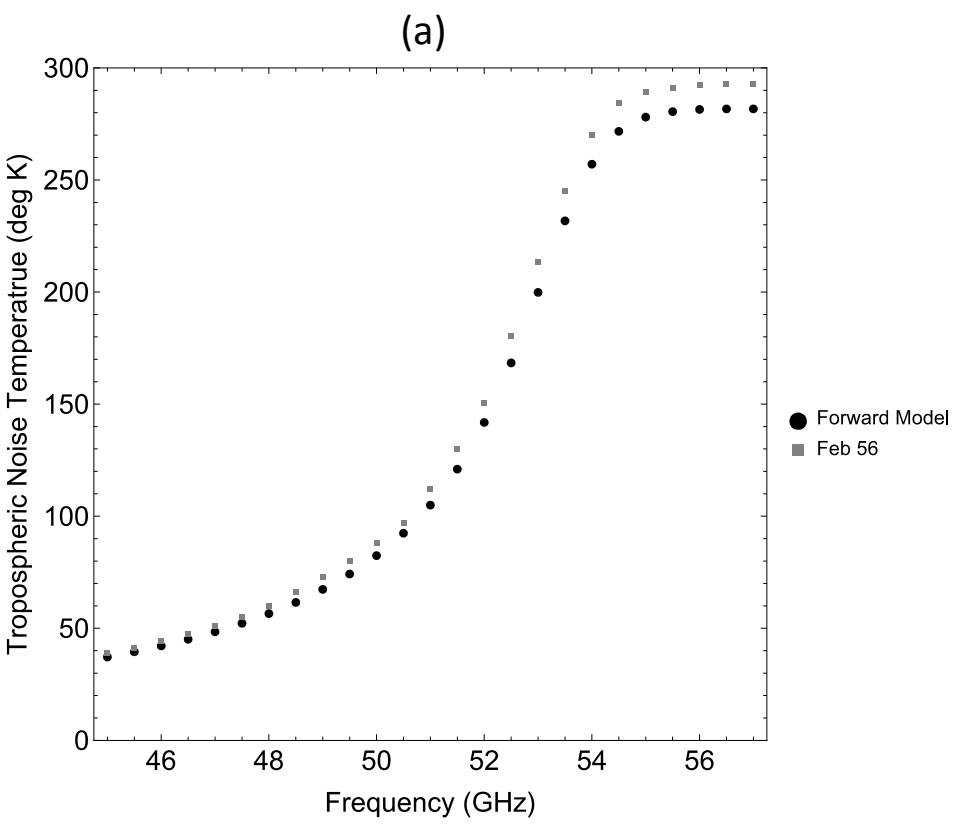
(a)
Tropospheric Noise Temperatrue (deg K)
300
250
200
150
100
50
0
46
48
50
52
54
56
Frequency (GHz)
Forward Model
Feb 56

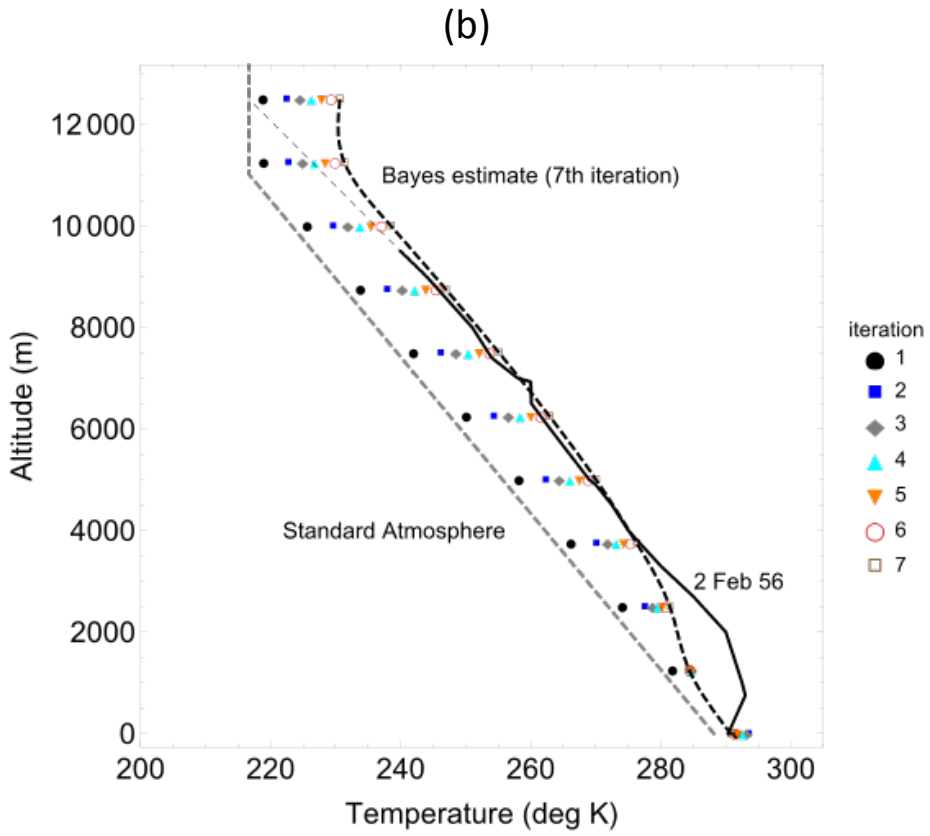
(b)
Altitude (m)
12 000
10 000
8000
6000
4000
2000
0
200
220
240
260
280
300
Temperature (deg K)
Bayes estimate (7th iteration)
Standard Atmosphere
2 Feb 56
iteration
1
2
3
4
5
6
7

Test case 1 Dakar: estimated temperature profile

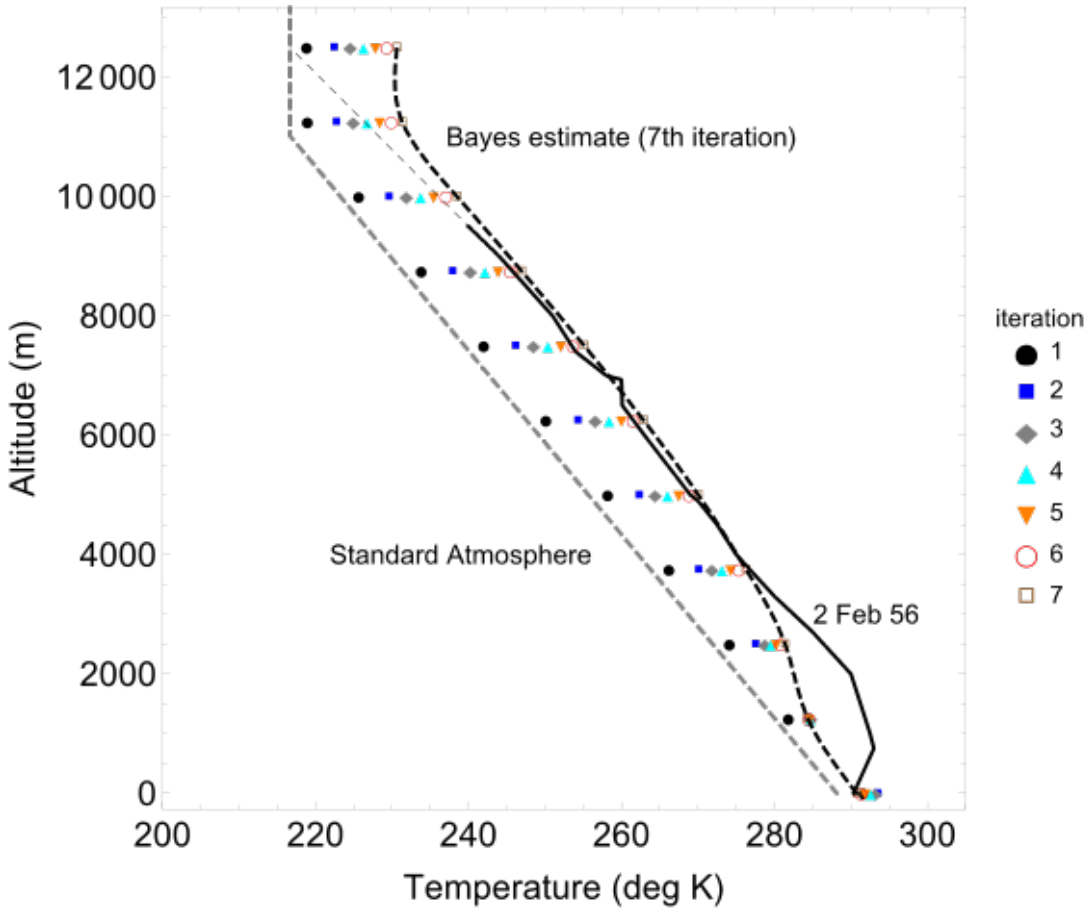

Discussion. The figure above shows the Bayes estimate of the atmospheric temperature profile using the 2 February 1956 Dakar brightness temperature data for the 52-57 GHz band. This band corresponds to the frequency range where absorption is changing most quickly. Seven iterations were performed as indicated in the figure. The thick dashed black line shows the spline curve for the 7th iteration. The solid black line is the radiosonde temperature profile. The thin gray line shows an extension of the sonde temperature profile into the Blake standard atmosphere. Note that the iterative solutions have converged and that Bayes procedure correctly estimates the on-scene measured surface temperature. Figure generated using ” *Brightness Temperature Dakar Senegal 2 February 1956 Actual Data.nb*”.

Test case 2: 7 December 2015 at the Stennis Airport

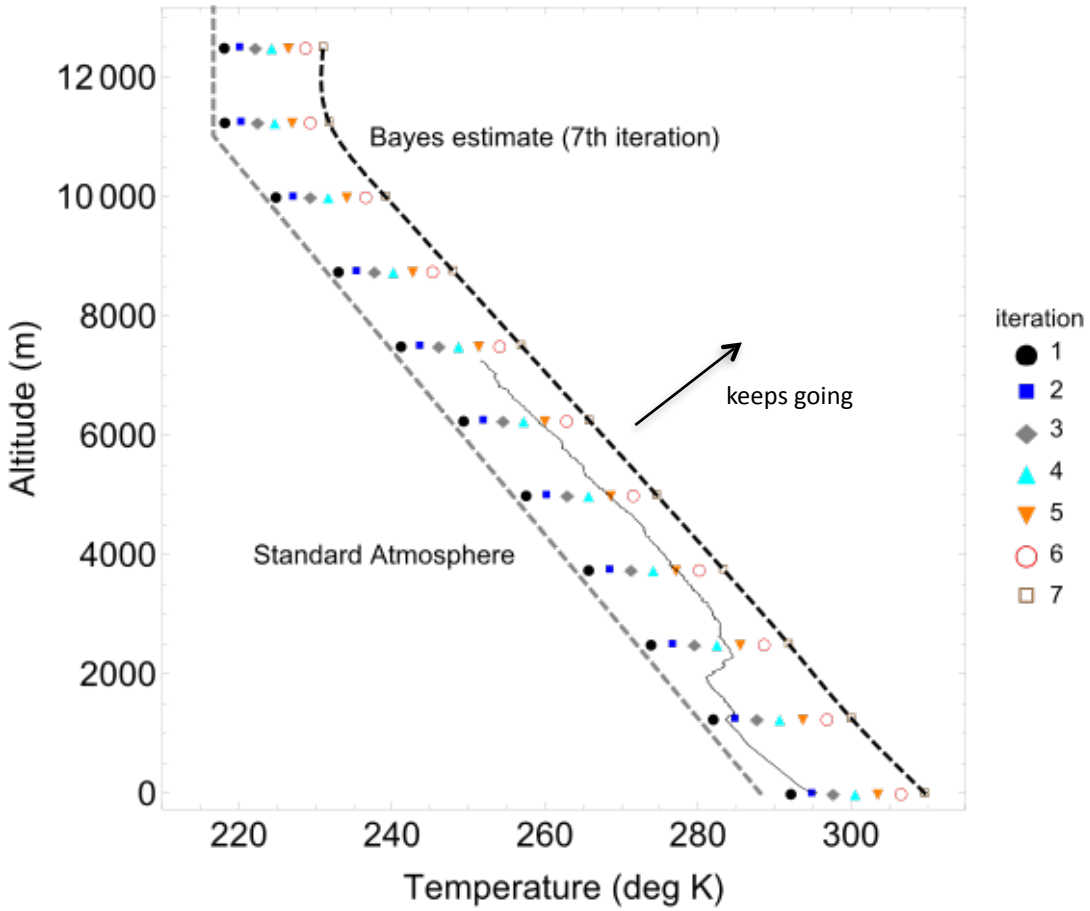

Discussion. The figure shows the Bayes estimate of the atmospheric temperature profile using 7 December 2015 brightness temperature data for the radar tilt angles in the 25-90 deg range. Seven iterations were performed as indicated in the figure. The thick dashed black line shows the spline curve for the 7th iteration. The solid black line is the sonde temperature profile. The thick, dashed gray line shows the Blake standard atmosphere. Note that the iterative solutions have not converged and that the Bayes procedure does not correctly estimate the on-scene measured surface temperature. The reason for this lack of convergence are discussed in the next slide. Figure generated using *" Brightness Temperature Dakar Senegal 2 February 1956 Actual Data.nb"*.

Information content and degrees of freedom

LOGLINEAR GROUP

Name at	Description	Case 1a	Case 1b	Case 2
		2 Feb 1956 52-57 GHz	2 Feb 1956 45-57 GHz	7 Dec 2015 25-90 deg at 33.4 GHz
Forward matrix **A** eigenvalues	$\lambda_1, \lambda_2, \lambda_3, \lambda_4$	3.003, 0.1827 0.008472, 2.204×10^{-4}	3.098, 0.2170 0.01037, 2.653×10^{-4}	0.0131, 3.35439×10^{-7} 1.4700×10^{-12}, 2.6930×10^{-18}
Degrees of freedom (d_s)	trace($\mathbf{A}_{avg}$)	0.9517	0.9750	0.0534
Information content (H)	$-1/2\log\lvert\mathbf{I}_{Nd}-\mathbf{A}_{avg}\rvert$	1.12949	1.17369	0.02745
Recognizable atmospheric states	2^H	2.28	2.26	1.02
Iterative solution convergence		Yes	Yes	No
Measures correct ground temp		Yes	Yes	No

Discussion. As indicated in the table shown above, there is significantly more information content in the Dakar 1956 data than in the 7 December 2015 data. It is the lack of information content in the 2015 data that leads to non convergence in the temperature estimation procedure. Also note that including the 45-52 Mhz data in the temperature estimate at the Dakar site does not improve the estimate. All of the useful information is in the 52-57 GHz band. The matrix $\mathbf{A}_{avg}$ shown in the above table is the averaging kernel matrix and is defined to be $\mathbf{A}_{avg}=(\mathbf{A}^T\mathbf{S}_\sigma^{-1}\mathbf{A}+\mathbf{S}_a^{-1})^{-1}\mathbf{A}^T\mathbf{S}_\sigma^{-1}\mathbf{A}$. Table generated using ” *Brightness Temperature Dakar Senegal 2 February 1956 Actual Data.nb*”.

Reference: Rogers, C.D. (2004), *Inverse Methods for Atmospheric Sounding: Theory and Practice* (Hackensack: World Scientific Publishing).

Conclusions

- The LLG radar can clearly track atmospheric temperature trends related to the radar receive brightness temperature (also called sky noise). Time scales at which the radar tracks changes span from hour to days. The shape of the radar receive brightness temperature as a function of radar elevation angle can be used to accurately calibrate the radar for the first time.
- A Bayesian procedure for estimating the atmospheric vertical temperature profile $T(z)$ from radar brightness temperature measurements at different elevation angles and operating frequencies has been developed. This procedure incorporates prior information about the environment and radar and combines it with brightness temperature data measured by the radar to produce sensible estimates of $T(z)$. The procedure also provides a computationally correct tool to support sophisticated radar design studies.
- The angular spectrum of the atmospheric brightness temperature at 33.4 GHz does not appear to have enough information content to allow the recovery of the atmospheric vertical temperature profile. This may not be the case at radar carrier frequencies that are located closer to 50-60 GHz where oxygen absorption is so important.
- Brightness temperature data previously collected by Westwater (1965) over the frequency range 45-57 GHz has been successfully inverted to produce a temperature profile that is in general agreement with the on-scene temperature profile measured by a radiosonde.

Possible tasks

LOGLINEAR GROUP

- Task 1 : Yanagisawa (1979) observed using a combination of 8.6 mm radar data and radiosonde data that the onset of positive vertical heat vertical heat flux in the atmosphere coincided with the observation of radar reflections from convective turbulence. We know that the LLG radar can measure the intensity of reflections from clear air turbulence at a very fine vertical scale. As this document shows, the radar has the potential to measure the vertical temperature profile at a coarse resolution (1 km). It may be possible to relate this to changes in vertical heat flux by incorporating information about the structure that the active portion of the radar detects. I do not know how to do this at the present but it is worth investigating.
  - **Reference**: Yanagisawa, Z. (1979) "Observation of Angle Echoes by 8.6-mm radar", Meteorology and Geophysics, Vol. 30, No. 3/4, November 1979.
- Task 2: Our radar can be used to monitor a parameter known as the the turbulent intensity. It is defined to be the ratio of the standard deviation of wind speed divided by the mean wind speed. Among other things it is a descriptor of the amount of slosh relative to the mean wind speed. It is used in the windmill industry to predict destructive loading effects on windmill blades. Detail on this can be found in Gasch (2012)
  - **Reference**: Gasch, R. and Twele,(2012) *Wind Power Plants* (Berlin: Springer Verlag).
- Task 3: Our radar can be used to constant in combination with extreme value theory to forecast the waiting time to any parameter that the radar measures. An obvious example here is wind gusts or bursts of abnormally high turbulent intensity. I have previously demonstrate how this can be done. A description can be found at the following:
  - http://demonstrations.wolfram.com/ExtremeValueForecasting/
- Task 4. Use the the brightness temperature that the radar observes in a change detection mode with the process initialized with a radiosonde launch.